JOURNAL OF PROPULSION AND POWER
Vol. 26, No. 3, May–June 2010

Reduced-Order Model for H_2O_2 Catalytic Reactor Performance Analysis

A. Pasini,* L. Torre,† L. Romeo,‡ A. Cervone,§ and L. d'Agostino¶
ALTA S.p.A., Ospedaletto, Pisa 56121, Italy

DOI: 10.2514/1.44355

The present paper describes a steady one dimensional model of the hydrogen peroxide decomposition flow in a pellet-type catalytic bed and its application to the parametric design of a typical reactor for small rocket propellant thrusters. The two-phase liquid-gas-vapor flow through the bed is treated as a homogeneous, adiabatic, chemically reacting flow, for which the properties depend on the local composition. Fast equilibrium hydrogen peroxide adsorption and first-order finite-rate desorption is assumed for the one-step hydrogen peroxide decomposition reaction on the catalyst surface. Standard viscous/aerodynamic correlations for porous media are used to account for pressure losses. The predictions of the model depend on a limited number of uncertain parameters, for which the values can be readily determined by comparison with the available experimental data. Good agreement has been attained between the model predictions and the results of hydrogen peroxide monopropellant thruster firings. The model provides a rational framework for identifying the main operational parameters of catalytic pellet beds, understanding their interactions, and efficiently guiding the reactor sizing and design, using the indications easily obtained from sensitivity analyses.

Nomenclature

A_{bed}	=	catalytic bed cross-section area
A_{f2}	=	Arrhenius preexponential factor
C	=	molar concentration
C_d	=	diffusion coefficient
C_f	=	friction coefficient
c_p	=	molar constant pressure specific heat
D_p	=	pellet diameter
E_{f2}	=	activation energy
e	=	molar internal energy
G	=	bed load
H	=	enthalpy
H_2O	=	water
H_2O_2	=	hydrogen peroxide
h	=	molar enthalpy
K_1	=	equilibrium adsorption constant
k_{b1}	=	backward adsorption constant
k_{f1}	=	forward adsorption constant
k_{f2}	=	forward desorption constant
L	=	catalytic bed length
$\mathcal{M}$	=	molecular weight
$\mathcal{M}_P$	=	mean product molecular weight
$\dot{m}$	=	propellant mass flow rate
N_s	=	number of active adsorption sites per unit volume of the catalytic bed
$\dot{n}$	=	molar flux per unit volume
O_2	=	oxygen
p	=	flow pressure
p_c	=	chamber pressure
p_{loss}	=	pressure losses
p_s	=	saturation pressure
p_v	=	pressure of H_2O_2 and H_2O vapors
q_v	=	heat of vaporization
$\mathcal{R}$	=	universal constant of gas
Re_p	=	pellet Reynolds number
$\dot{r}$	=	molar concentration
S	=	catalytic surface
Sc	=	Schmidt number
S_p	=	overall surface of the pellets
T	=	flow temperature
T_c	=	chamber temperature
T_{do}	=	dryout temperature
T_{end}	=	exit flow temperature
$\boldsymbol{u}$	=	flow velocity
$\dot{V}$	=	volumetric flow rate
Y	=	H_2O_2 mass concentration
α	=	void fraction
Δ_p	=	pressure drop
ε	=	molar evaporation fraction parameter
$\tilde{\varepsilon}$	=	bed porosity
θ	=	relative occupancy of the adsorption sites
λ	=	decomposition parameter
μ	=	dynamic viscosity
$\boldsymbol{\tau}$	=	viscous stress tensor
ν	=	kinematic viscosity
ν_j	=	j-th stoichiometric coefficient

Subscripts

end	=	catalytic bed end section
g	=	gaseous
i	=	initial condition
j	=	general element
l	=	liquid
p	=	pellet

Presented as Paper 2008-5025 at the 44td AIAA/ASME/SAE/ASEE Joint Propulsion Conference, Hartford, CT, 21–23 July 2008; received 13 March 2009; revision received 5 Oct. 2009; accepted for publication 4 Nov. 2009.

*Project Engineer, Via Gherardesca 5; currently Ph.D. Student, Department of Aerospace Engineering, Via Diotisalvi, Pisa University, Pisa 56100, Italy; a.pasini@alta-space.com. Member AIAA.

†Project Manager, Via Gherardesca 5; l.torre@alta-space.com. Member AIAA.

‡Project Engineer, Via Gherardesca 5; l.romeo@alta-space.com. Member AIAA.

§Project Manager, Via Gherardesca 5; a.cervone@alta-space.com. Member AIAA.

¶Via Gherardesca 5; currently Professor, Department of Aerospace Engineering, Via Diotisalvi, Pisa University, Pisa 56100, Italy; luca.dagostino@ing.unipi.it. Member AIAA.

Superscripts

(i)	=	initial condition
$''$	=	products
$'$	=	reactants
$^\circ$	=	standard condition
(s)	=	on the catalytic surface

I. Introduction

IN RECENT years high concentration or rocket grade hydrogen peroxide (HTP) has received increased attention as a storable oxidizer for space propulsion applications due to its low toxicity and relative ease of use. For the development of efficient HTP thrusters, it is necessary to attain almost complete decomposition of the propellant by optimally matching the operating parameters of the thruster (chamber pressure, HTP concentration, mass flow rate, and feed pressure) and the configuration of the catalytic bed, which depends on the propellant dwell time and load, on the choice of the active catalytic species, as well as on the characteristics of the support in terms of chemical nature (metallic, ceramic, etc.), shape (screens, grids, pellets, or monoliths), porosity, and specific surface area.

The development of reduced-order models capable of rapidly predicting the performance of catalytic beds, conducting parametric analyses, and providing interpretative indications for the preliminary sizing and design of liquid propellant rocket thrusters is of special interest to space engineers. However, not many such models have been proposed so far, probably due to the difficulty of adequately describing the complex two-phase, chemically reacting, liquid-gas-vapor flow through the catalytic bed. Satterfield et al. [1] have examined the catalytic decomposition of H_2O_2 in a tubular reactor from an analytical standpoint. A numerical simulation of the catalytically decomposing flow of H_2O_2 through a silver screen bed has been reported by Chiappetta et al. [2]. The flow is assumed to be axisymmetric, with pressure losses modeled by means of Darcy's law for porous media. The H_2O_2 decomposition kinetics is represented by a one-step chemical reaction, in which the preexponential constant in the Arrhenius law is assumed to vary linearly with catalyst bed surface-to-volume ratio and the corresponding activation energy is set to a constant value of 12 kcal/mol (50232 J/mol). Corpening et al. [3] investigated the thermal decomposition of liquid HTP injected in a hot stream of hydrogen peroxide (HP) decomposition products. Their model assumes steady, 1-D adiabatic flow and accounts for droplet evaporation, gas phase decomposition kinetics, and the mass, momentum, and energy conservation laws for the two phases.

None of these works, however, specifically refers to the HTP decomposition through pellet bed reactors, which is the focus of the present paper. By introducing suitable simplifications, the mass, momentum, and energy conservation equations for the reacting flow through a pellet bed reactor are specialized into a system of two first-order, coupled, quasi-linear ordinary differential equations (ODEs) for the pressure and reaction advancement parameter, for which the solution for the imposed values of the inlet properties of the HTP flow allows to determine the evolution of the entire flow as a function of the distance from the inlet section of the catalytic bed. The model predictions are found to depend on a limited number of uncertain parameters, for which the values can be iteratively determined by comparison with the available experimental data using standard Bayesian system identification methods. The model provides in this way a rational framework for identifying the main operational parameters of catalytic pellet beds, understanding their interactions, and efficiently guiding the preliminary reactor sizing and design based on the indications readily obtained from sensitivity analyses. The following sections illustrate in detail the development of this process with reference to the application of the proposed model to the reconstruction of the experimental results obtained by Torre et al. [4] from recent firing tests of a 5 N HTP monopropellant thruster prototype.

II. Reacting Flow Model in the Catalytic Pellet Bed

A. Homogeneous Two-Phase Flow Model

With reference to Fig. 1, a given mass flux

$$\dot{m} = \dot{n}^{(i)}_{H_2O_2(l)}\mathcal{M}_{H_2O_2} + \dot{n}^{(i)}_{H_2O(l)}\mathcal{M}_{H_2O}$$

of HTP solution enters the bed in liquid form at specified values of pressure p_i, temperature T_i, and H_2O_2 mass concentration Y; gets in contact with the catalytic spheres; and decomposes into oxygen and steam according to the global reaction:

$$H_2O_2 \rightarrow H_2O + \frac{1}{2}O_2 - 98.2 \text{ kJ/mol}$$

originating a flow with local composition:

$$\dot{n}_{H_2O_2}(\lambda) = \dot{n}^{(i)}_{H_2O_2} - \lambda = \frac{Y\dot{m}}{\mathcal{M}_{H_2O_2}} - \lambda;$$

$$\dot{n}_{H_2O}(\lambda) = \dot{n}^{(i)}_{H_2O} + \lambda = \frac{(1-Y)\dot{m}}{\mathcal{M}_{H_2O}} + \lambda \quad \text{and} \quad \dot{n}_{O_2}(\lambda) = \frac{1}{2}\lambda$$

The exothermic H_2O_2 decomposition increases the local temperature, first heating the liquid flow up to the boiling conditions corresponding the local value of the pressure and then progressively evaporating both the H_2O_2 and the H_2O contained in the HTP propellant. The resulting two-phase liquid-gas-vapor flow in the bed is treated as a homogeneous, adiabatic, chemically reacting flow, for which the properties depend on the local composition, assumed equal in both phases, and on the advancement of the evaporation process from $\varepsilon = 0$ (pure liquid) to 1 (pure gas). Oxygen dissolution in the liquid phase, as well as the velocity and temperature slips between the two phases, are neglected.

From Dalton's law, the partial pressure of oxygen is

$$p_{O_2} = \frac{\dot{n}_{O_2}}{\dot{n}_{O_2} + \varepsilon(\dot{n}_{H_2O_2} + \dot{n}_{H_2O})}\,p$$

as a function of the molar evaporation fraction ε. For simplicity, the partial pressures of H_2O_2 and H_2O are approximated as the products of the partial fractions in the liquid times the saturation pressures at the mixture temperature, and, therefore, in the assumption of equal composition of the two phases

$$p_{H_2O_2(g)} = \frac{\dot{n}_{H_2O_2}}{\dot{n}_{H_2O_2} + \dot{n}_{H_2O}}\,p_{sH_2O_2}(T) \quad \text{and}$$

$$p_{H_2O(g)} = \frac{\dot{n}_{H_2O}}{\dot{n}_{H_2O_2} + \dot{n}_{H_2O}}\,p_{sH_2O}(T)$$

Substituting in the expression of the mixture pressure $p = p_{O_2} + p_{H_2O_2(g)} + p_{H_2O(g)}$ one obtains

$$\left[1 - \frac{\dot{n}_{O_2}}{\dot{n}_{O_2} + \varepsilon(\dot{n}_{H_2O_2} + \dot{n}_{H_2O})}\right]p = \frac{\dot{n}_{H_2O_2}p_{sH_2O_2}(T) + \dot{n}_{H_2O}p_{sH_2O}(T)}{\dot{n}_{H_2O_2} + \dot{n}_{H_2O}} = p_v(T,\lambda)$$

Hence, at the bed inlet ($\dot{n}_{O_2} = 0$)

$$p_i \geq p_v(T_i, 0) \Rightarrow T \leq T_b(p_i) \qquad \text{(inlet boiling temperature)}$$

while at the conclusion of the evaporation ($\varepsilon = 1$)

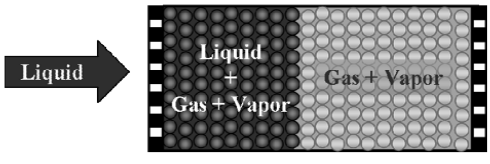

Fig. 1 Qualitative flow path inside the catalytic bed.

$$p \le \frac{\dot{n}_{H_2O_2} + \dot{n}_{H_2O} + \dot{n}_{O_2}}{\dot{n}_{H_2O_2} + \dot{n}_{H_2O}} p_v(T,\lambda) \Rightarrow T \ge T_{do}(p,\lambda)$$

(dry-out temperature)

For $T_i < T < T_{do}$ the (adiabatic) enthalpy balance of the mixture at any axial location in the bed

$$\begin{aligned}
&\dot{n}_{O_2}[h^\circ_{O_2} + c_{pO_2}(T - T^\circ)] + \varepsilon\{\dot{n}_{H_2O_2}[h^\circ_{H_2O_2(g)} \\
&\quad + c_{pH_2O_2(g)}(T - T^\circ)] + \dot{n}_{H_2O}[h^\circ_{H_2O(g)} + c_{pH_2O(g)}(T - T^\circ)]\} \\
&\quad + (1-\varepsilon)\{\dot{n}_{H_2O_2}[h^\circ_{H_2O_2(l)} + c_{pH_2O_2(l)}(T - T^\circ)] + \dot{n}_{H_2O}[h^\circ_{H_2O(l)} \\
&\quad + c_{pH_2O(l)}(T - T^\circ)]\} = \dot{n}^{(i)}_{H_2O_2}[h^\circ_{H_2O_2(l)} + c_{pH_2O_2(l)}(T_i - T^\circ)] \\
&\quad + \dot{n}^{(i)}_{H_2O}[h^\circ_{H_2O(l)} + c_{pH_2O(l)}(T_i - T^\circ)]
\end{aligned}$$

determines $\varepsilon = \varepsilon(T,\lambda) < 1$, and substitution of this result in the preceding equation for $p_v(T,\lambda)$ implicitly determines the temperature $T = T(p,\lambda)$. On the other hand, for $T > T_{do}$ the liquid is fully evaporated ($\varepsilon = 1$), and the preceding energy balance can be solved explicitly for the mixture temperature $T = T(\lambda)$ (the pressure is uninfluential in the present perfect gas approximation).

With these results, the volumetric fluxes of the two phases are

$$\dot{V}_l = (1-\varepsilon)\frac{\dot{n}_{H_2O_2}\mathcal{M}_{H_2O_2}}{\rho_{H_2O_2(l)}} + (1-\varepsilon)\frac{\dot{n}_{H_2O}\mathcal{M}_{H_2O}}{\rho_{H_2O(l)}} \quad \text{and}$$

$$\dot{V}_g = [\dot{n}_{O_2} + \varepsilon(\dot{n}_{H_2O_2} + \dot{n}_{H_2O})]\frac{\mathcal{R}T}{p}$$

and all of the relevant properties of the homogeneous reacting mixture: 1) concentrations

$$C_{H_2O_2} = \frac{\dot{n}_{H_2O_2}}{\dot{V}_l + \dot{V}_g}; \qquad C_{H_2O} = \frac{\dot{n}_{H_2O}}{\dot{V}_l + \dot{V}_g};$$

$$C_{O_2} = \frac{\dot{n}_{O_2}}{\dot{V}_l + \dot{V}_g} \quad \text{and} \quad C = \frac{\dot{n}_{H_2O_2} + \dot{n}_{H_2O} + \dot{n}_{O_2}}{\dot{V}_l + \dot{V}_g}$$

2) density and void fraction

$$\rho = \frac{\dot{n}_{H_2O_2}\mathcal{M}_{H_2O_2} + \dot{n}_{H_2O}\mathcal{M}_{H_2O} + \dot{n}_{O_2}\mathcal{M}_{O_2}}{\dot{V}_l + \dot{V}_g} \quad \text{and} \quad \alpha = \frac{\dot{V}_g}{\dot{V}_l + \dot{V}_g}$$

3) viscosities

$$\mu \cong \mu_l(1-\alpha) + \mu_g\alpha \quad \text{and} \quad \nu = \frac{\mu}{\rho}$$

4) constant pressure specific heat

$$c_p = \frac{\dot{n}_{H_2O_2}c_{pH_2O_2} + \dot{n}_{H_2O}c_{pH_2O} + \dot{n}_{O_2}c_{pO_2}}{\dot{n}_{H_2O_2} + \dot{n}_{H_2O} + \dot{n}_{O_2}} \quad \text{with}$$

$$\begin{cases} c_{pH_2O_2} = (1-\varepsilon)c_{pH_2O_2(l)} + \varepsilon c_{pH_2O_2(g)} \\ c_{pH_2O} = (1-\varepsilon)c_{pH_2O(l)} + \varepsilon c_{pH_2O(g)} \end{cases}$$

can be determined as functions of the local values of the pressure p and the reaction advancement parameter λ.

B. Reaction Model

Fast equilibrium adsorption and first-order finite-rate product desorption are assumed for the one-step H_2O_2 decomposition reaction on the catalyst surface S:

$$H_2O_2 + S \underset{k_{b1}}{\overset{k_{f1}}{\rightleftarrows}} S\text{-}H_2O_2(ad) \overset{k_{f2}}{\rightarrow} H_2O + \frac{1}{2}O_2$$

Therefore, indicating with $C^{(s)}$ the relevant molar concentrations on the catalytic surface, with N_s the number of active adsorption sites per unit volume of the catalytic bed and with θ the relative occupancy of the adsorption sites, from the reactant adsorption equilibrium condition:

$$k_{f1}C^{(s)}_{H_2O_2}N_s(1-\theta) = k_{b1}N_s\theta \quad \text{one obtains} \quad \theta = \frac{K_1C^{(s)}_{H_2O_2}}{1 + K_1C^{(s)}_{H_2O_2}}$$

where $K_1 = k_{f1}/k_{b1}$ the adsorption equilibrium constant. Similarly, from the product desorption kinetics, the volumetric reaction rate is

$$\dot{r} = k_{f2}N_s\theta = A_{f2}e^{-E_{f2}/\mathcal{R}T}N_s\frac{K_1C^{(s)}_{H_2O_2}}{1 + K_1C^{(s)}_{H_2O_2}}$$

where A_{f2} is the Arrhenius preexponential constant and E_{f2} the corresponding activation energy.

Standard viscous/aerodynamic correlations for porous media (Ergun [5]) are used to account for pressure losses:

$$\frac{dp_{loss}}{dx} = \left(150\frac{1-\tilde{\varepsilon}}{Re_p} + 1.75\right)\frac{1-\tilde{\varepsilon}}{\tilde{\varepsilon}^3}\frac{\rho u^2}{D_p} \quad \text{with} \quad Re_p = \frac{uD_p}{\nu}$$

where p_{loss} is the pressure loss, x the streamwise coordinate, $\tilde{\varepsilon}$ the bed porosity, u the nominal cross-sectional flow velocity (i.e., evaluated for unit bed porosity), and D_p is the (spherical) pellet diameter.

C. Governing Equations

Application of the pertinent governing equations to steady, 1-D, adiabatic, homogeneous, creeping flow between two neighboring axial stations of a catalytic bed with constant cross-sections gives 1) mixture continuity equation

$$\oint_S \rho\boldsymbol{u}\cdot d\boldsymbol{S} = 0 \Rightarrow \frac{d(\rho u)}{dx} = 0 \Rightarrow \rho u = G \equiv \text{constant} \Rightarrow u = \frac{G}{\rho}$$

2) species continuity equation

$$\oint_S C_j\boldsymbol{u}\cdot d\boldsymbol{S} = \int_V (\nu''_j - \nu'_j)\dot{r}\,dV \Rightarrow \frac{d(C_ju)}{dx} \cong u\frac{dC_j}{dx} = (\nu''_j - \nu'_j)\dot{r}$$

3) axial momentum equation

$$\begin{aligned}
\oint_S \rho\boldsymbol{u}\boldsymbol{u}\cdot d\boldsymbol{S} &= -\oint_S p\,d\boldsymbol{S} + \oint_S \boldsymbol{\tau}\cdot d\boldsymbol{S} \Rightarrow \rho u\frac{du}{dx} \\
&= -\frac{dp}{dx} - \frac{dp_{loss}}{dx} \cong 0
\end{aligned}$$

while the adiabatic energy equation with formation energy contributions and negligible viscous dissipation

$$\oint_S \rho h_t\boldsymbol{u}\cdot d\boldsymbol{S} = 0 \Rightarrow \rho u\frac{dh_t}{dx} = 0 \Rightarrow h_t \equiv \text{constant}$$

has already been used. Hence, from the general expression of composition changes

$$dC_j = \frac{d\dot{n}_j}{\dot{V}_l + \dot{V}_g} = \frac{\nu''_j - \nu'_j}{\dot{V}_l + \dot{V}_g}\,d\lambda$$

and from preceding results, the relevant initial value problem (IVP) for the reacting flow through the catalytic pellet bed can be expressed

$$\frac{d\lambda}{dx} = \frac{\dot{V}_l + \dot{V}_g}{u}A_{f2}e^{-E_{f2}/\mathcal{R}T}N_s\frac{K_1C^{(s)}_{H_2O_2}}{1 + K_1C^{(s)}_{H_2O_2}} \quad \text{with} \quad \lambda(0) = 0$$

$$\frac{dp}{dx} = -\left(150\frac{1-\tilde{\varepsilon}}{Re_p} + 1.75\right)\frac{1-\tilde{\varepsilon}}{\tilde{\varepsilon}^3}\frac{\rho u^2}{D_p} \quad \text{with} \quad p(0) = p_i$$

Together with the preceding expressions for the flow velocity, density, viscosity, evaporation, and temperature, the preceding two ODEs for the local composition and pressure can be numerically integrated to determine the evolution of the flow as a function of the distance from the inlet section.

D. Diffusion Effects

For design purposes it is quite important to assess whether the operation of a catalytic pellet bed is limited by mass diffusion effects because, in this case, any improvement of the surface reaction kinetics would be rather ineffective in increasing the bed performance. The similarity of transport phenomena provides a simple approximate way to attain this objective. For a viscous and diffusive boundary layer on a flat plate, the generalized Reynolds analogy between mass and momentum transport on the wall surface can be expressed by the ratio of the nondimensional diffusion coefficient and the corresponding local value of the friction coefficient:

$$\frac{C_d}{C_f} = \frac{\dot{m}_j^{(s)}/\rho u(Y_j - Y_j^{(s)})}{2\tau^{(s)}/\rho u^2} \approx \frac{1}{2}\mathrm{Sc}^{-1/2} \cong \frac{1}{2}$$

Here the Schmidt number $\mathrm{Sc} = \nu/\mathcal{D}$ is assumed equal to 1 (not unrealistic approximation for most fluids [6]) and the friction coefficient C_f can be (very conservatively) estimated by attributing to the viscous friction on the pellet surface S_p all of the preceding bed pressure losses (which include instead both viscous and aerodynamic components):

$$\frac{\mathrm{d}p_{\mathrm{loss}}}{\mathrm{d}x} = \left(150\frac{1-\varepsilon}{Re_p} + 1.75\right)\frac{1-\varepsilon}{\varepsilon^3}\frac{\rho u^2}{D_p} = C_f\frac{1}{2}\rho u^2\frac{1}{A}\frac{\mathrm{d}S_p}{\mathrm{d}x}$$

where for tetrahedral packing of the spherical pellets with diameter D_p in a bed of cross-sectional area A:

$$\frac{1}{A}\frac{\mathrm{d}S_p}{\mathrm{d}x} = \frac{\pi\sqrt{2}}{D_p} \Rightarrow C_d \cong \frac{1}{\pi\sqrt{2}}\left(150\frac{1-\tilde{\varepsilon}}{Re_p} + 1.75\right)\frac{1-\tilde{\varepsilon}}{\tilde{\varepsilon}^3}$$

As a consequence, the mass flux of reactants at the catalyst surface is

$$= \tilde{\dot{m}}_{\mathrm{H_2O_2}}^{(s)} = C_d\rho u(Y_{\mathrm{H_2O_2}} - Y_{\mathrm{H_2O_2}}^{(s)})\frac{1}{A}\frac{\mathrm{d}S_p}{\mathrm{d}x}$$

$$= C_d\rho u(Y_{\mathrm{H_2O_2}} - Y_{\mathrm{H_2O_2}}^{(s)})\frac{\pi\sqrt{2}}{D_p}\mathcal{M}_{\mathrm{H_2O_2}}\dot{r}$$

The mass fraction $Y_{\mathrm{H_2O_2}}^{(s)}$ of H_2O_2 on the catalytic surface can be expressed in terms of the molar concentration $C_{\mathrm{H_2O_2}}^{(s)}$ using the equimass diffusion condition in the fluid phase to/from the impermeable catalytic surface (s):

$$Y_{\mathrm{H_2O_2}}^{(s)} = \frac{\mathcal{M}_{\mathrm{H_2O_2}}C_{\mathrm{H_2O_2}}^{(s)}}{\mathcal{M}_{\mathrm{H_2O_2}}C_{\mathrm{H_2O_2}}^{(s)} + \mathcal{M}_P(C - C_{\mathrm{H_2O_2}}^{(s)})}$$

Finally, substitution of the expressions of $Y_{\mathrm{H_2O_2}}^{(s)}$ and $\dot{r}$ as functions of $C_{\mathrm{H_2O_2}}^{(s)}$ in the preceding equation gives:

$$C_d\rho u\left[Y_{\mathrm{H_2O_2}} - \frac{\mathcal{M}_{\mathrm{H_2O_2}}C_{\mathrm{H_2O_2}}^{(s)}}{\mathcal{M}_{\mathrm{H_2O_2}}C_{\mathrm{H_2O_2}}^{(s)} + \mathcal{M}_P(C - C_{\mathrm{H_2O_2}}^{(s)})}\right]\frac{\pi\sqrt{2}}{D_p}$$

$$= \mathcal{M}_{\mathrm{H_2O_2}}A_{f2}e^{-E_{f2}/\mathcal{R}T}N_s\frac{K_1C_{\mathrm{H_2O_2}}^{(s)}}{1 + K_1C_{\mathrm{H_2O_2}}^{(s)}}$$

from which $C_{\mathrm{H_2O_2}}^{(s)}$ and, therefore, the influence of diffusive effects can be estimated.

III. Model Results and Discussion

The model has been fitted on the test data of the first of a series of monopropellant firings using the FC-LR-87 platinum-based catalyst (Torre et al. [4], Romeo et al. [7]). In particular, the uncertain parameters related to the geometric characteristics of the bed (the bed porosity $\tilde{\varepsilon}$ and the number of active sites per unit bed volume N_s) and to the reaction kinetics (the Arrhenius preexponential factor A_{f2}, the activation energy E_{f2} and the equilibrium constant K_1) have been chosen by matching the model predictions of the bed pressure drop and outlet temperature to the corresponding test measurements.

Table 1 Model settings and results compared with the reference bed configuration and firing

	Reference bed configuration and firing results	Model
Catalyst	FC-LR-87 ($Pt/\alpha - Al_2O_3$)	FC-LR-87 ($Pt/\alpha - Al_2O_3$)
Propellant	85.7% HP	85.7% HP
Pellet diameter	0.6 mm	0.6 mm
Bed diameter	18 mm	18 mm
Bed length	60 mm	60 mm
Bed load	19.02 kg/s m^2	19.02 kg/s m^2
Mass flow rate	4.84 g/s	4.84 g/s
Chamber pressure	17.65 bar	17.64 bar
Chamber temperature	831 K	830 K
Catalytic bed pressure drop	0.65 bar	0.63 bar
Advancement parameter	-	94.80%

Good agreement has been attained between the observed data and the model results, as illustrated Table 1. It may also be noticed in support of the validity of the preceding approach that this procedure has led to a value of the bed porosity equal to 0.40, in good agreement (Kaviany [8]) with the bulk porosity of well shaken spherical packing ($0.36 \leq \tilde{\varepsilon} \leq 0.43$) and to a realistic value of the activation energy ($E_{f2} = 18124$ J/mol) of the desorption rate constant [9].

Figure 2 shows the axial profiles of the H_2O_2 decomposition advancement parameter and of the flow temperature and the pressure predicted by the model as functions of the distance from the propellant inlet section for the reference configuration of the catalytic bed summarized in Table 1. The temperature profile of Fig. 2 clearly shows the presence of three different regions. In the first region the HTP entering the bed gets in contact with the catalytic spheres and starts decomposing into oxygen and steam, generating the rapid increase of the flow temperature up to the local boiling conditions (region I). In the second region the saturation temperature corresponding to the local value of the pressure is reached and the vaporization of the liquid starts to occur. During this phase the absorption of the latent heat of vaporization essentially stabilizes the flow temperature, generating the flat portion of the temperature profile (region II). The very small decline of the flow temperature reflects the dependence of the saturation temperature on the local pressure, which is slowly decreasing as a consequence of the flow losses through the bed. The simplified assumption of simultaneous evaporation of H_2O_2 and H_2O results in just one nearly isothermal vaporization process instead of the dual-step profile obtained by

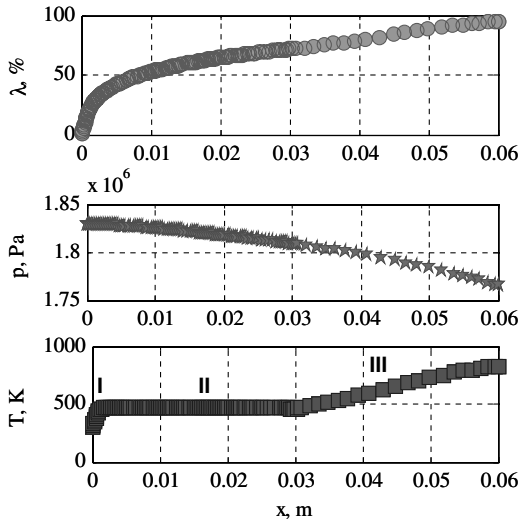

Fig. 2 Axial profiles of reaction advancement parameter and flow pressure and temperature predicted by the model for the reference catalytic bed configuration of Table 1.

Zhou and Hitt [10], assuming separate successive evaporation of H_2O and H_2O_2. Clearly, neither of these approaches is exact because they both ignore the solution of the mutual equilibrium of the two liquids. However, the error introduced by the present approximation is considered acceptable in consideration of the intrinsic accuracy of the model because it only modifies the HTP evaporation profile without significantly affecting the overall latent heat absorbed by the process which controls the attainment of dryout conditions and influences the flow conditions at the bed outlet. At the end of the evaporation of the liquid ($\varepsilon = 1$), the flow is completely gaseous (dryout conditions), and the heat developed by the further decomposition of H_2O_2 tends to asymptotically increase the flow temperature up to the adiabatic equilibrium HTP decomposition temperature (region III), which depends on the initial composition and, to a more limited extent, also on the flow pressure. As indicated by the slope of the pressure profile in Fig. 2, the flow losses monotonically increase along the bed together with the flow velocity as a consequence of the HTP decomposition reaction, for which the advancement reduces the flow density by first sustaining the evaporation of the liquid and later by raising the gas flow temperature. The advanced parameter reaches about 94% of the adiabatic equilibrium value, indicating that the reference bed configuration did not allow for complete H_2O_2 decomposition, in accordance with the results of firing tests.

Figure 3 reports the molar concentration profiles of the reactants and products of the HTP decomposition in the axial direction along the catalytic bed. There is no significant difference between the mean local concentration of these species and the corresponding concentrations on the catalytic surface estimated by means of the simplified treatment of mass diffusion effects (Sec. II.D). Hence, it appears that the reference configuration of the catalytic bed operates under finite-rate kinetics conditions, suggesting that improvements of the catalytic activity should have a significant impact on the bed performance. This conclusion is fully consistent with the results of firing tests recently carried out on a number of catalysts with different decomposition activities (Pasini et al. [11], Torre et al. [4]).

As mentioned in the introduction, the proposed model also represents a useful tool for understanding the role and mutual relationships of the main parameters involved in the preliminary design of catalytic pellet beds. To illustrate this point, the figures from 4–8 show the parametric influences of the pellets diameter D_p, the bed loading G, the bed length L, the chamber pressure p_c and the H_2O_2 mass composition Y of the HTP propellant on the advanced parameter λ, the bed pressure drop Δ_p, and the bed exit temperature T_{end}. All of these results have been computed using the estimated values of the kinetics properties and bulk porosity of the reference FC-LR-87 catalyst bed configuration.

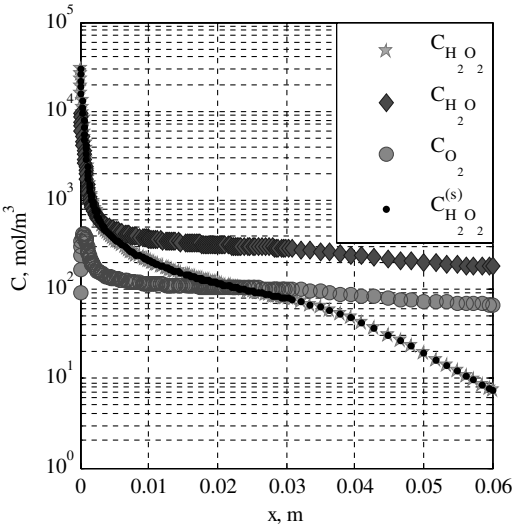

Fig. 3 Molar concentrations of the reacting species along the bed length.

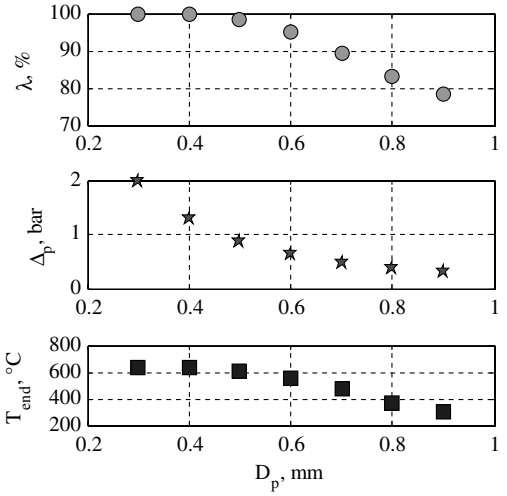

Fig. 4 Advancement parameter λ, pressure drop Δ_p, and exit temperature T_{end} as functions of the pellet sphere diameter D_p for the following bed operating conditions and configuration: $G = 19.02$ kg/m^2 s, $p_c = 17.65$ bar, $\dot{m} = 4.84$ g/s, $Y = 0.857$, and $L = 60$ mm.

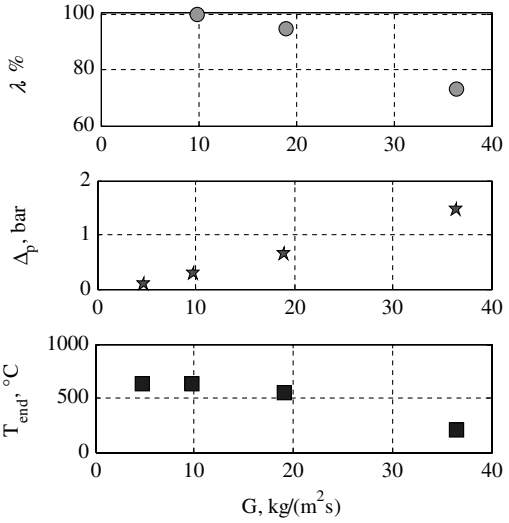

Fig. 5 Advancement parameter λ, pressure drop Δ_p, and exit temperature T_{end} as functions of the bed loading G for the following bed operating conditions and configuration: $p_c = 17.65$ bar, $\dot{m} = 4.84$ g/s, $Y = 0.857$, $D_p = 0.6$ mm and, $L = 60$ mm.

The analysis of Fig. 4 indicates that even a moderate reduction of the pellet diameter from 0.6 to 0.4 mm is expected to have a positive effect on the H_2O_2 decomposition reaction, raising the advanced parameter close to 100%. This improvement is clearly linked to the larger active surface of the catalyst, but probably also to the increase of the bed pressure drop, which in the present setup favors the completion of the decomposition reaction by increasing the mean operational pressure of the catalytic bed at the constant value of the propellant mass flow rate controlled by the cavitating venturi mounted on the HTP supply line. On the other hand, for pellet diameters higher than 0.8 mm the bed pressure drop approaches an almost constant value because the given bed length becomes insufficient for completing the isothermal vaporization phase (region II).

The reduction of the bed load, which in the present operational conditions at constant mass flow rate corresponds to an increase of the bed cross-sectional area, yields a rapid improvement of the advanced parameter and a drastic reduction of the bed pressure drop (see Fig. 5). The second effect cannot be considered a real advantage because it implies a reduction of the fluid dynamic dissipation in the catalytic reactor and a parallel increase of the danger of the onset of flow instabilities.

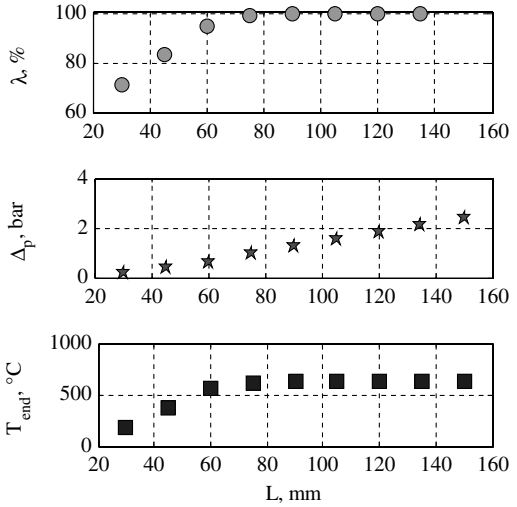

Fig. 6 Advancement parameter λ, pressure drop Δ_p, and exit temperature T_{end} as functions of the bed length L for the following bed operating conditions and configuration: $G = 19.02$ kg/m^2 s, $p_c = 17.65$ bar, $\dot{m} = 4.84$ g/s, $Y = 0.857$, $D_p = 0.6$ mm, and $L = 60$ mm.

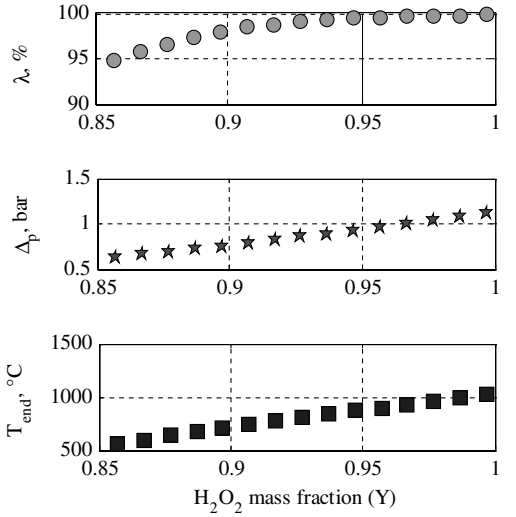

Fig. 8 Advancement parameter λ, pressure drop Δ_p, and exit temperature T_{end} as functions of the H_2O_2 mass fraction Y for the following bed operating conditions and configuration: $G = 19.02$ kg/m^2 s, $p_c = 17.65$ bar, $\dot{m} = 4.84$ g/s, $Y = 0.857$, $D_p = 0.6$ mm, and $L = 60$ mm.

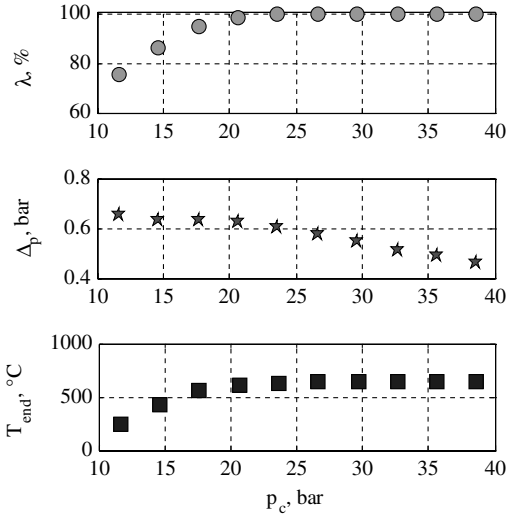

Fig. 7 Advancement parameter λ, pressure drop Δ_p, and exit temperature T_{end} as functions of the chamber pressure p_c for the following bed operating conditions and configuration: $G = 19.02$ kg/m^2 s, $\dot{m} = 4.84$ g/s, $Y = 0.857$, $D_p = 0.6$ mm, and $L = 60$ mm.

The increase of the catalytic bed length above the reference value $L = 60$ mm affects the HTP dwell time by promoting the completion of the decomposition reaction (see Fig. 6). Also in this case the increased pressure losses have the same beneficial effect as for the reduction of the pellet diameter.

The effects of the variation of the pressure in the chamber downstream of the catalytic bed are illustrated in Fig. 7. This pressure affects the mean operational pressure of the catalytic bed; high pressures promote the completion of the reaction by reducing the bed length required for the vaporization of the liquid, thereby extending the next phase of H_2O_2 decomposition in the gas phase. This effect is confirmed by the temperature profiles of Fig. 9, computed at very different values of the chamber pressure. Higher pressures in the catalytic bed also increase the mean density of the gaseous mixture, resulting in a reduced flow velocity and pressure losses (see Fig. 7).

Finally, Fig. 8 indicates that the level of completion of the H_2O_2 decomposition reaction increases with the initial H_2O_2 mass fraction of the HTP propellant, most likely as a consequence of the acceleration of the chemical kinetics at the higher temperatures developed in the catalytic bed.

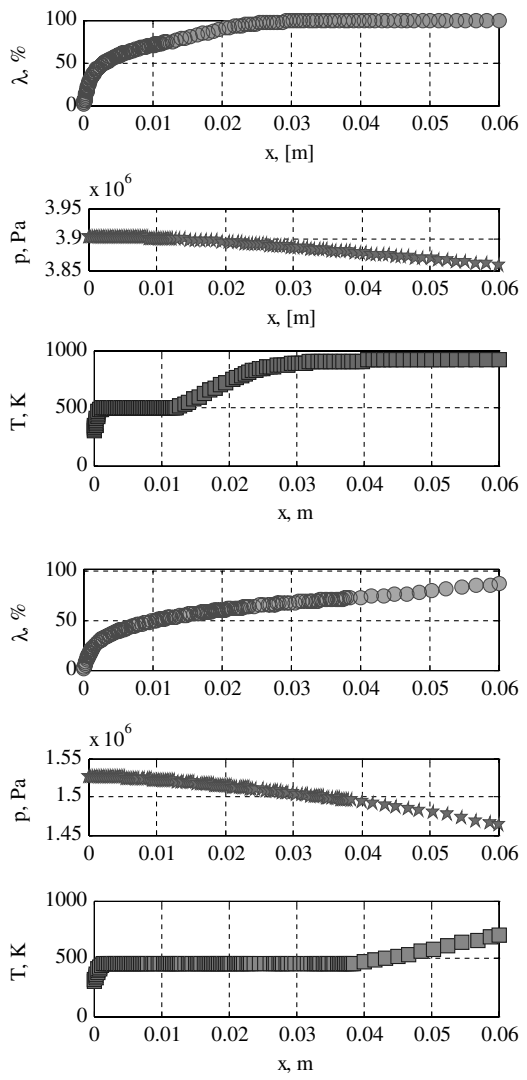

Fig. 9 Advancement parameter, pressure, and temperature profiles for high ($p_c = 38.65$ bar, top) and low ($p_c = 14.65$ bar, bottom) chamber pressures for the following bed operating conditions and configuration: $G = 19.02$ kg/m^2 s, $\dot{m} = 4.84$ g/s, $Y = 0.857$, $D_p = 0.6$ mm, and $L = 60$ mm.

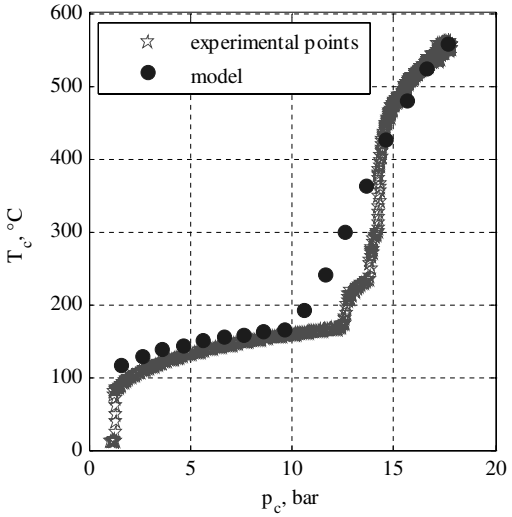

Fig. 10 Chamber temperature T_c as a function of the chamber pressure p_c, experimentally measured during a monopropellant firing and predicted by the model.

The prediction capabilities of the model have been tested by plotting the temperature T_{end} as a function of the corresponding pressure p_{end} at the exit of the catalytic bed. In Fig. 10 the model results have been compared with the quasi-steady measurements of the downstream chamber temperature T_c and pressure p_c obtained during the evolution of the monopropellant thruster firing used for matching the free parameters of the model. The initial part of the curve, characterized by a moderately increasing temperature and a relatively large pressure rise, corresponds to the evaporation of the liquid at increasing temperatures during the initial pressurization of the thruster. The second part of the curve, up to $T \cong 450$°C, corresponds to the very rapid transient of the gas mixture temperature soon after the conclusion of the evaporation of the liquid. Finally, the last portion of the curve corresponds to the relatively slow approach to the asymptotic operational conditions of the thruster, due to the thermal contact of the decomposing flow with the walls of the catalytic bed chamber. Not surprisingly, the largest discrepancies between the predictions of the present steady model and the experimental results occur in the central region of the temperature vs pressure curve, corresponding to the most rapid transient response of the flow through the catalytic bed. In the other regions of the curve in Fig. 10, in which the flow evolution is more nearly quasi static, good agreement is attained, confirming the validity of the proposed model.

IV. Conclusions

The proposed reduced-order model has been developed with the aim of better understanding the mutual relationships between the main operational parameters of catalytic pellet reactors for H_2O_2 decomposition in monopropellant rocket thruster applications, as well as for deducing quantitative information for design development orientation. Both of these objectives have been successfully met because the model clearly highlights the role of the main factors affecting the catalytic bed performance in these kinds of applications, and its demonstrated capability of predicting the influence of pellets size, bed loading, bed length, downstream chamber pressure, and H_2O_2 mass concentration in the HTP propellant allows for effectively guiding the tradeoff of the most important design parameters relevant to the design development of a given catalyst/support combination for a specific rocket thruster application.

On the basis of the parametric analyses generated by the proposed model, the following conclusions can be drawn.

The reduction of the pellets size favors the completion of the decomposition reaction in two ways: by increasing the active catalytic surface per unit bed volume and by raising the operational pressure of the reactor, thus accelerating its catalytic activity. Hence, small pellets sizes are effective for reducing the bed volume while still preserving acceptable performance. Additionally, the increase of the pressure drop through the catalytic bed and the reduction of its volume by favoring a more rapid initial pressurization of the reactor also improve the typical raise time of the thrust, a crucial aspect in space propulsion applications.

The bed length and load (which varies inversely with the bed cross section) affect the propellant dwell time in the reactor. For a given value of the dwell time, high aspect ratio beds develop higher flow losses and have the earlier mentioned advantage of favoring a more rapid initial pressurization of the reactor, at the cost of some reduction of the steady-state total pressure for nozzle expansion. However, an excessive reduction of the bed load, in the attempt to increase the thrust chamber pressure, reduces the fluid dynamic damping in the bed, exposing the chamber to the risk of development of self-sustained flow oscillations. The present steady model is clearly incapable of predicting unsteady effects in the bed but can provide useful indications for the choice of the bed pressure drop and chamber pressure levels most suited for steady-state thruster operation.

The pressure of the catalytic bed accelerates the reaction kinetics and represents, therefore, an effective operational parameter for completing the decomposition of H_2O_2 in shorter beds. When operating at constant propellant mass flow rate, the increase of the chamber pressure reduces both the liquid evaporation phase and the flow velocity, extending the dwell time and reducing the bed pressure losses. All of these effects add to the preceding one, making the chamber pressure level a crucial parameter for improving the performance of HTP monopropellant thrusters.

The predicted irrelevance of mass diffusion effects on the catalytic reaction represents a very significant indication of the proposed model. If confirmed, it simply implies that any further improvements of the decomposition kinetics must rely on more efficient catalyst/substrate combinations (not a simple task to achieve at their present state of development).

According to the results of the proposed model, the catalytic bed for the reference monopropellant thruster application could attain almost complete H_2O_2 decomposition at design HTP mass flow rate by the following ways: 1) decreasing the pellets size from 0.6 mm to 0.4 mm, 2) halving the bed load to 10 $\text{kg}/\text{m}^2\,\text{s}$, 3) increasing the bed length from 60 to 80 mm, 4) increasing the nominal chamber pressure up to 23 bar, 5) using HTP with 97% H_2O_2 composition by weight, or by suitable combinations of the above.

Based on the predictions of the proposed model, the authors became convinced of the need of 1) introducing very significant reductions of the pellet diameter and bed volume without decreasing the overall catalytic surface, 2) limiting the excessive increase of the bed pressure drop and increasing the reaction kinetics by raising the chamber pressure, 3) selecting the chamber length-to-diameter ratio to secure sufficiently rapid initial pressurization of the reactor.

It appears, therefore, that the design tradeoff of catalytic pellet beds for HTP monopropellant thrusters also involves consideration of the transient operation and response, which are not predicted by the present model. Therefore, the authors have now undertaken the development of such an unsteady model, with the specific aim of generating useful design information on the initial pressurization transient and on the influence of nonadiabatic effects and bed preheating on the steady-state and intermittent pulsed operation of monopropellant thrusters.

Acknowledgments

The authors gratefully acknowledge the support of the Italian Ministry for Production Activities. The authors would like to express their gratitude to Fausto Calderazzo, Daniela Belli Dell'Amico, Mariano Andrenucci, Fabrizio Paganucci, and Renzo Lazzeretti of University of Pisa, Pisa, Italy, for their constant and friendly encouragement.

References

[1] Satterfield, C. N., Resnick, H., and Wentworth, R. L., "Simultaneous Heat and Mass Diffusion in a Diffusion-Controlled Chemical Reaction: Part 1—Studies in a Tubular Reactor," *Chemical Engineering Progress*,

Vol. 50, 1954, pp. 460–466.
[2] Chiappetta, L. M., Spadaccini, L. J., and Huang, H., "Modeling a Hydrogen Peroxide Gas Generator for Rockets," AIAA Paper 2000-3223, 17–19 July 2000.
[3] Corpening, J. H., Heister, S. D., Anderson, W. E., and Austin, B. J., "A Model for Thermal Decomposition of Hydrogen Peroxide," AIAA Paper 2004-3373, 11–14 July 2004.
[4] Torre, L., Pasini, A., Romeo, L., and d'Agostino, L., "Firing Performances of Advanced Hydrogen Peroxide Catalytic Beds in a Monopropellant Thruster Prototype," AIAA Paper 2008-5575, 20–23 July 2008.
[5] Ergun, S., "Fluid Flow Through Packed Columns," *Chemical Engineering Progress*, Vol. 48, American Institute of Chemical Engineers, New York, 1952, pp. 89–94.
[6] Cussler, E. L., *Diffusion: Mass Transfer in Fluid Systems*, Cambridge University Press, New York, 1984, pp. 439–469.
[7] Romeo, L., Pasini, A., Torre, L., d'Agostino, L., and Calderazzo, F., "Comparative Characterization of Advanced Catalytic Beds in a Hydrogen Peroxide Thruster Prototype," AIAA Paper 2008-5575, 20–23 July 2008.
[8] Kaviany, M., "Flow in Porous Media," *The Handbook of Fluid Dynamics*, edited by R. W. Johnson, CRC Press LLC, Boca Raton, FL, 1998, pp. 8–10.
[9] Bramanti, C., Cervone, A., d'Agostino, L., Musker, A. J., and Saccoccia, G., "Experimental Characterization of Advanced Materials for Catalytic Decomposition of Hydrogen Peroxide," AIAA Paper 2006-5238, 9–12 July 2006.
[10] Zhou, X., and Hitt, D. L., "One-Dimensional Modeling of Catalyzed H_2O_2 Decomposition in Microchannel Flows," AIAA Paper 2003-3584, 23–26 June 2003.
[11] Pasini, A., Torre, L., Romeo, L., d'Agostino, L., Cervone, A., and Musker, A., "Experimental Characterization of a 5 N Hydrogen Peroxide Monopropellant Thruster Prototype," AIAA Paper 2007-5464, 8–11 July 2007.

D. Talley
Editor in Chief